Joint Seismic Inversion and Wavelet Estimation Using Physics-Informed Neural Networks

1st Anthony João Bet
Departamento de Informática e Estatística
Universidade Federal de Santa Catarina
Florianópolis, Brasil
ORCID 0009-0000-1619-3482

2nd Rafael Santiago
Departamento de Informática e Estatística
Universidade Federal de Santa Catarina
Florianópolis, Brasil
ORCID 0000-0001-7033-125X

3rd Bruno Barbosa Rodrigues
Petrobras
Rio de Janeiro, Brasil
ORCID 0000-0002-6127-8212

4th Mauro Roisenberg
Departamento de Informática e Estatística
Universidade Federal de Santa Catarina
Florianópolis, Brasil
mauro.roisenberg@ufsc.br
ORCID 0000-0001-9707-0360

***Abstract*—Seismic inversion, used to estimate elastic and petrophysical properties of subsurface regions to identify potential oil and gas reservoirs, is a challenging, ill-posed, and highly nonlinear problem. Neural networks have shown great potential in addressing these challenges due to their ability to model complex nonlinear relationships. However, their application often requires a large amount of training data, which is often a limiting factor in practical applications. In this work, we propose a Physics-Informed Neural Network (PINN) architecture for seismic inversion and wavelet estimation. The seismic wavelet is an essential parameter to be applied in the forward seismic physical model to obtain the seismic traces from impedance values, so determining its correct value is critical. The novelty of our approach lies in the introduction of a network designed to estimate the seismic wavelet, trained jointly with the inversion network. We evaluated the model on the well-known Marmousi2 synthetic dataset and on real poststack seismic data. Results demonstrate that the model outperforms traditional approaches while accurately estimating the wavelet. On the real dataset, the results indicate the framework's robustness and its ability to generalize to complex geological scenarios, highlighting the potential of PINNs in geophysical applications.**

***Index Terms*—Seismic Inversion, Machine Learning, Oil and Gas, Physics Informed neural Networks, Neural Networks, Wavelet Estimation**

I. Introduction

Seismic inversion aims to estimate the elastic and petrophysical properties of subsurface rocks from seismic data, typically involving a nonlinear mapping between observed data and model parameters.

Neural networks are well-suited for this task due to their ability to approximate complex nonlinear relationships, improving inversion accuracy and efficiency compared to conventional approaches [1], [2]. However, their application is often limited by the need for large labeled datasets, typically derived from well logs, which are scarce and costly to obtain in practice [2], [3], [4], [5], [6].

This project is sponsored by Petrobras under CT number 0050.0122221.22.9

Physics-Informed Neural Networks (PINNs) address this limitation by incorporating physical knowledge directly into the training process. By embedding physical laws as constraints, PINNs guide the learning process toward physically consistent solutions, reducing reliance on labeled data and improving convergence [1], [3]. Additionally, PINNs enable the estimation of unknown parameters of the physical model itself, such as petrophysical properties [7].

In seismic inversion, many PINN-based approaches incorporate physics through a forward convolutional model [1], [7], [8], [9]. These methods typically require a predefined seismic wavelet, which is feasible in synthetic scenarios but becomes a limitation in real-world applications where the wavelet is unknown and must be estimated separately.

In this work, we propose a Physics-Informed Neural Network framework that jointly performs acoustic impedance inversion and seismic wavelet estimation. By treating the wavelet as a trainable variable within a convolutional forward model, the proposed approach enables a unified and physically consistent inversion process.

The main contributions of this work are:

- A PINN architecture for acoustic seismic inversion that enables automatic wavelet estimation under limited labeled data;
- Improved performance over a standard data-driven neural network on both synthetic and real datasets.

The remainder of this paper is organized as follows. Section II reviews related work. Section III presents the theoretical formulation and methodology. Section IV describes the experimental setup and results. Finally, Section V concludes the paper and outlines future directions.

II. Related Works

Physics can be incorporated into neural networks through different strategies depending on data availability and prior knowledge. When large datasets are available but the underlying physics is partially unknown, physical consistency can be encouraged through data-driven approaches such as symmetry-based augmentation. Conversely, when the governing physics is well understood but data is scarce, architectures can be designed to embed physical structure, as in graph neural networks. Physics-Informed Neural Networks (PINNs) provide a hybrid approach by incorporating physical constraints—typically through additional loss terms such as PDE residuals—making them particularly suitable for inverse problems with limited labeled data [1], [3].

PINNs have been increasingly applied to geophysical problems, including petrophysical inversion and wave propagation. Prior works demonstrate their effectiveness in estimating subsurface properties from indirect measurements [10], improving training efficiency through adaptive sampling strategies [11], and recovering wave velocities in complex Full Waveform Inversion (FWI) scenarios [12]. These studies highlight the robustness of PINNs in handling heterogeneous media and limited data regimes.

In seismic inversion, physics-informed approaches commonly incorporate forward seismic modeling as a constraint during training. For example, [8] showed that embedding a convolutional forward model improves impedance estimation compared to purely data-driven methods. Extensions combining PINNs with Bayesian inference further enable uncertainty quantification in inversion results [7], [9], enhancing their applicability in real-world scenarios.

Despite these advances, most existing methods assume a predefined seismic wavelet, which is often unavailable in practice and must be estimated separately. This limitation motivates the present work, which proposes a PINN framework that jointly estimates acoustic impedance and the seismic wavelet within a unified, physically consistent formulation.

III. THEORY AND METHODS

This section presents the theoretical formulation and methodological framework of the proposed Physics-Informed Neural Network (PINN) for seismic inversion, including the problem formulation, network architecture, physical constraints, and multi-objective loss.

A. Problem Formulation

The inversion problem consists of estimating model parameters $\mathbf{m}$ from measurements $\mathbf{d}$, related through a physical operator $\mathcal{F}$:

$$\mathbf{d} = \mathcal{F}(\mathbf{m}) + \mathbf{e}, \tag{1}$$

where $\mathbf{e}$ represents measurement noise.

In a data-driven approach, a neural network $\mathcal{G}$ is trained to approximate the inverse mapping $\mathcal{F}^{-1}$:

$$\hat{\mathbf{m}} = \mathcal{G}(\mathbf{d}; \boldsymbol{\theta}), \tag{2}$$

where $\boldsymbol{\theta}$ denotes the learnable parameters. In this work, $\mathbf{d}$ corresponds to seismic data and $\mathbf{m}$ to acoustic impedance.

To improve generalization and enforce physical consistency, PINNs incorporate the forward operator $\mathcal{F}$ as a regularization constraint, minimizing the mismatch between observed data $\mathbf{d}$ and synthetic data $\hat{\mathbf{d}}$ reconstructed from the predicted model:

$$\hat{\mathbf{d}} = \mathcal{F}(\hat{\mathbf{m}}) = \mathcal{F}(\mathcal{G}(\mathbf{d}; \boldsymbol{\theta})). \tag{3}$$

This formulation constrains the model to satisfy both the observed data and the underlying physical laws. The operator $\mathcal{F}$ is detailed in Section III-C.

B. Network Architecture

The proposed architecture (Figure 1), inspired by [8], consists of four main modules: (i) a Sequential Block with GRU layers to capture temporal dependencies; (ii) a Local Pattern Block with 1D convolutions to extract local features; (iii) a Regression Block mapping features to acoustic impedance; (iv) a Wavelet Block that predicts the wavelet spectrum and phase ϕ.

The outputs of the Sequential and Local Pattern blocks are summed and fed into two branches: the Regression Block for impedance estimation and the Wavelet Block for wavelet prediction. The latter includes a Gaussian smoothing layer with trainable standard deviation σ, and the wavelet phase is also learned as a parameter.

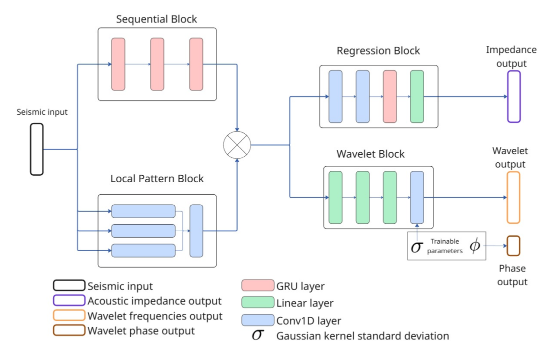

Fig. 1. Proposed architecture. Seismic input is processed by GRU-based (temporal) and convolutional (local) blocks, whose outputs are combined and fed into two branches: impedance regression and wavelet estimation. The wavelet branch predicts the spectrum and phase, followed by Gaussian smoothing.

The wavelet estimation block begins with a flattening operation followed by three linear layers (500, 100, and N_f units), where N_f is the number of frequency samples of the wavelet spectrum W_f. This depends on the wavelet duration T_w and sampling interval dt:

$$N_t = \left\lfloor \frac{T_w}{dt} \right\rfloor. \tag{4}$$

Due to symmetry in the Fourier transform of real signals, only half of the spectrum is required:

$$N_f \leftarrow \begin{cases} (N_t/2) + 1, & \text{if } N_t \text{ is even} \\ (N_t + 1)/2, & \text{if } N_t \text{ is odd} \end{cases} \tag{5}$$

A final 1D convolution with a Gaussian kernel (size 5) smooths the spectrum, attenuating high-frequency noise. All parameters, including σ and ϕ, are optimized jointly during training.

The next section describes how these outputs are incorporated into the loss function.

C. Forward Model and Physical Consistency

To enforce physical consistency, the seismic response is simulated within the training pipeline using the physical operator $\mathcal{F}$, enabling learning from unlabeled data.

The operator $\mathcal{F}$ is implemented as a convolution between a wavelet and reflection coefficients, defined as the Forward Convolutional Model (F_c). Reflection coefficients (RC) are computed from the predicted acoustic impedance using the normal-incidence equation [13]:

$$RC(t, AI) = \frac{\mathrm{AI}(t + \Delta t) - \mathrm{AI}(t)}{\mathrm{AI}(t + \Delta t) + \mathrm{AI}(t)}, \quad (6)$$

where AI denotes acoustic impedance.

The synthetic seismic is then obtained by convolving the RC traces with the predicted wavelet:

$$\hat{\mathbf{d}} = F_c(W_t, \hat{\mathbf{m}}) = W_t * RC \quad (7)$$

where $*$ denotes convolution and W_t is the time-domain wavelet obtained via IFFT of the spectrum W_f (Figure 2).

The seismic misfit is defined as:

$$L_s = \sum_{\mathbf{d_u} \in U} MSE(F_c(W_t, \hat{\mathbf{m}}_\mathbf{u}), \mathbf{d_u}), \quad (8)$$

where U is the set of unlabeled seismic traces.

To promote physically realistic wavelets, a spectral regularization term is introduced:

$$L_w = \sum_{i=1}^{N_f} \frac{i-1}{N_f - 1} \cdot p(f_i), \quad (9)$$

where f_i are frequency components and $p(\cdot)$ is a probability function. This term penalizes high-frequency components, encouraging low-frequency spectra consistent with real seismic wavelets.

By incorporating F_c through L_s and L_w, the model is constrained to produce physically consistent impedance and wavelet estimates while leveraging large amounts of unlabeled seismic data.

D. Multi-Objective Loss Function

The model is trained using a multi-objective loss:

$$L_t = \alpha L_p + \beta L_s + \gamma L_w, \quad (10)$$

where the property loss is defined as:

$$L_p = \sum_{(\mathbf{d_l}, \mathbf{m_l}) \in L} MSE(\mathcal{G}(\mathbf{d_l}), \mathbf{m_l}), \quad (11)$$

with L denoting labeled seismic–impedance pairs.

The weights are set as $\alpha = 1$, $\beta = \frac{|L|}{|U|}$, and $\gamma = 0.1\frac{|L|}{|U|}$, balancing contributions from labeled and unlabeled data.

Each term has a specific role: L_p enforces supervised impedance learning, L_s constrains seismic reconstruction, and L_w regularizes the wavelet spectrum. Since L_s and L_w depend only on unlabeled data, they enhance learning beyond the limited labeled set.

Model parameters are optimized via backpropagation to minimize L_t. The training workflow is illustrated in Figure 2.

E. Metrics

The models are evaluated using the Pearson correlation coefficient (PCC), the coefficient of determination (R^2), and the mean structural similarity index (M-SSIM). M-SSIM is computed as the average SSIM over image blocks.

IV. EXPERIMENTS AND RESULTS

This chapter presents the experimental setup and evaluates the performance of the proposed PINN framework on both synthetic and real seismic datasets, comparing its results with a conventional neural network to assess accuracy, robustness, and physical consistency.

A. Synthetic Case Experiments

The synthetic dataset used in this work is *Marmousi2* [14]. Impedance data are converted to time, and synthetic seismic is generated from acoustic impedance (AI).

Reflection coefficients (RC) are computed using Equation 6, followed by convolution with an Ormsby wavelet (5–10–60–89 Hz). Gaussian white noise (15 dB) is added to simulate measurement noise. The resulting dataset contains 13,601 traces with 950 samples, spanning 17 km and 1.898 s.

For training, 10 seismic–impedance pairs were selected to simulate well logs (8 for training, 2 for testing). To increase variability, trace 2300 (around 3000 m) was manually included. A total of 10,000 traces were used as unlabeled data.

The wavelet duration was set to $T_w = 0.2$ s and the sampling interval to $dt = 2 \times 10^{-3}$ s, yielding $N_f = 51$ (Equation 5).

Figure 3 shows the predicted impedance over all traces. The model reproduces the main geological features, although lateral continuity is limited due to the use of 1D convolutions, which process traces independently [8].

Figure 4 shows predictions on test traces, with strong agreement with ground truth ($PCC = 0.97$, $R^2 = 0.85$), except for small deviations after 1.75 s.

Setting $\beta = 0$ reduces the model to a standard neural network (NN). Table I shows that the PINN outperforms the NN across all metrics.

Figure 5 shows the seismic reconstructed from the estimated wavelet, with high similarity to the reference ($M\text{-}SSIM = 0.95$), indicating consistency with the imposed physical constraints.

Figure 6 compares the estimated and true wavelets. The predicted wavelet accurately captures both shape and phase (difference $< 0.1°$), with a similar spectral distribution.

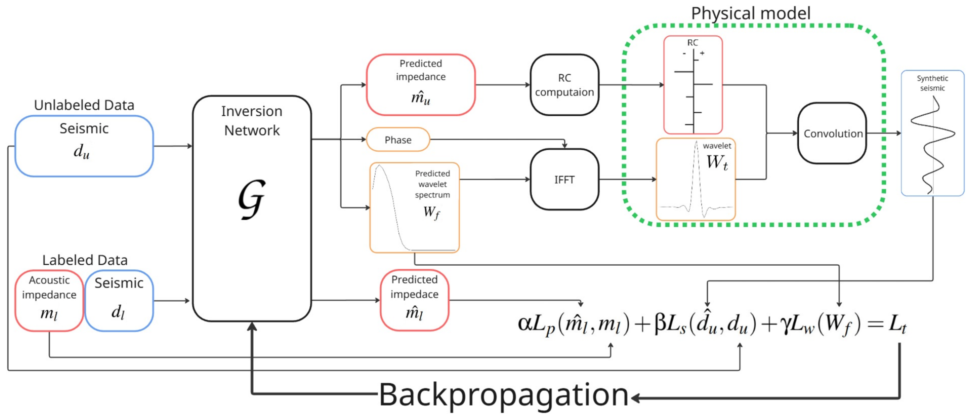

Fig. 2. Training workflow of the proposed PINN. Labeled and unlabeled data are used to predict impedance and wavelet parameters. Synthetic seismic generated through the forward model enables computation of L_s and L_w, while L_p is computed from labeled data. The combined loss L_t is used for optimization.

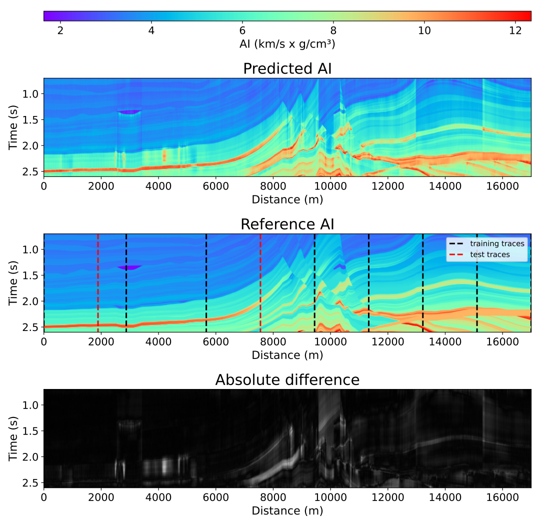

Fig. 3. Acoustic inversion on the *Marmousi2* dataset: (i) predicted impedance, (ii) reference impedance, and (iii) absolute difference. The model captures the main structures with localized discrepancies.

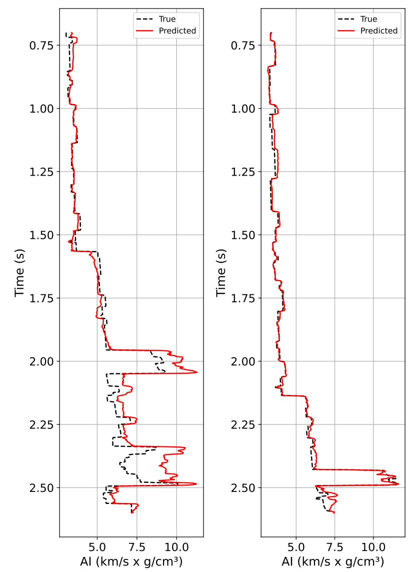

Fig. 4. Predicted vs. true impedance in test traces, showing high correlation ($PCC = 0.97$, $R^2 = 0.85$).

TABLE I

MODEL PERFORMANCE ON THE SYNTHETIC DATASET. PCC AND R^2 ARE COMPUTED ON TEST TRACES, AND M-SSIM ON FULL IMPEDANCE MAPS.

Metric	NN	PINN
PCC	0.76	0.97
R^2	0.55	0.85
M-SSIM	0.24	0.84

B. Real Case Experiments

The model was evaluated on real poststack seismic data and acoustic impedance well logs. The dataset consists of a 2D seismic section with 683 traces and a two-way time (TWT) of 0.5 s. All traces were used as unlabeled data. Four well logs were used as labeled data: three for training/validation and one for testing.

Figure 7 shows the inversion results for the PINN. The PINN produces less noisy results with improved lateral continuity. Compared with the seismic data (Figure 10), the PINN better delineates reflectors. Quantitative results (Table II) obtained via 3-fold cross-validation confirm that the PINN outperforms the NN.

TABLE II

MODEL COMPARISON USING 3-FOLD CROSS-VALIDATION.

Metric	NN	PINN
PCC	0.51	0.65
R^2	0.11	0.24

Figure 8 presents the test trace results. The PINN achieves higher accuracy ($PCC = 0.89$, $R^2 = 0.79$) compared to the NN ($PCC = 0.58$, $R^2 = 0.20$).

Figure 10 compares predicted and real seismic data. The

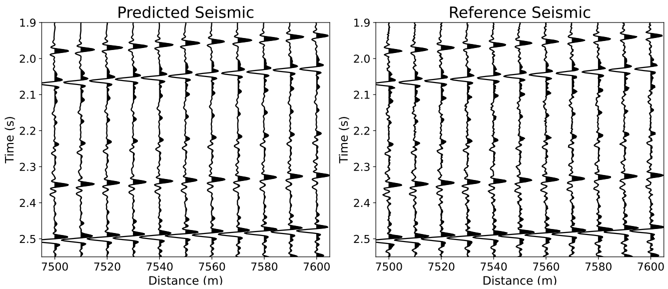

Fig. 5. Predicted vs. reference seismic data, showing high similarity ($M\text{-}SSIM = 0.95$).

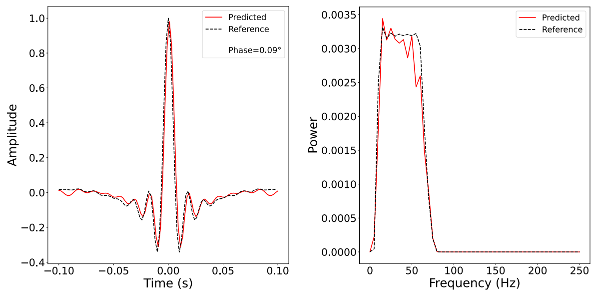

Fig. 6. Comparison of reference and predicted wavelets (left) and spectra (right). The model recovers both phase and spectral characteristics with high accuracy.

results show strong visual similarity ($M\text{-}SSIM = 0.75$), although localized reductions in similarity along reflector boundaries suggest minor phase discrepancies.

Figure 9 shows the estimated wavelet and spectrum. The spectrum is dominated by low-frequency components (below 40 Hz, peak around 15 Hz), consistent with typical seismic wavelets. The estimated phase is $8.2°$.

C. Hardware and Software

The models were trained on an NVIDIA GeForce GTX 1080 Ti GPU. All software was implemented in Python, using the PyTorch, NumPy, and scikit-learn libraries. In the synthetic experiment, PINN training takes approximately 30 minutes, whereas the standard NN requires about 1 minute. In the real-case experiment, both PINN and NN training take approximately 30 seconds. Code is available at [15].

V. Conclusion

Seismic inversion is a key method for modeling subsurface properties in oil and gas exploration. While neural networks have shown strong potential for addressing complex and ill-posed problems, their performance is limited by the scarcity of well log data. Physics-Informed Neural Networks (PINNs) mitigate this issue by incorporating prior physical knowledge into training, reducing dependence on labeled data. Recent PINN-based approaches leverage convolutional forward models as physical constraints, but most require prior wavelet modeling or extraction by specialists.

This work proposes a PINN framework for acoustic seismic inversion that integrates the convolutional forward model and enables automatic wavelet estimation during training. By removing the need for prior wavelet modeling, the approach reduces expert dependency and simplifies the inversion workflow. The model was evaluated on the synthetic *Marmousi2* dataset and a real poststack dataset, outperforming non-PINN models in both cases with minimal labeled data. In the synthetic case, the model accurately recovers the wavelet, while in the real dataset it estimates realistic low-frequency

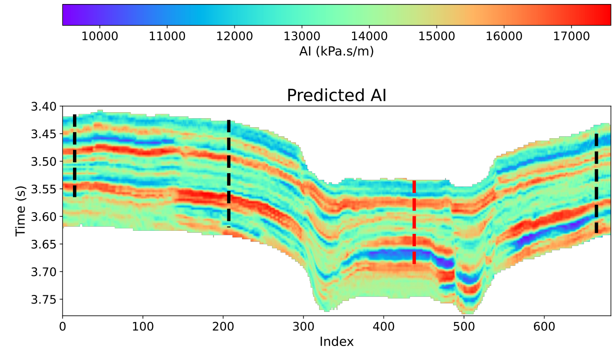

Fig. 7. Acoustic inversion on real data. Solid black lines indicate horizons of the zone of interest, dashed black lines indicate training wells, and the dashed red line indicates the test well.

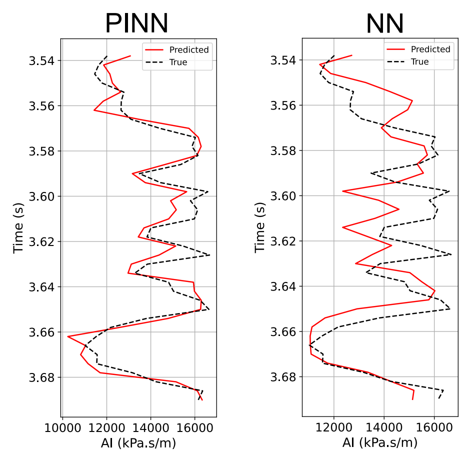

Fig. 8. Test trace comparison between PINN (left) and NN (right). The PINN shows superior agreement with ground truth.

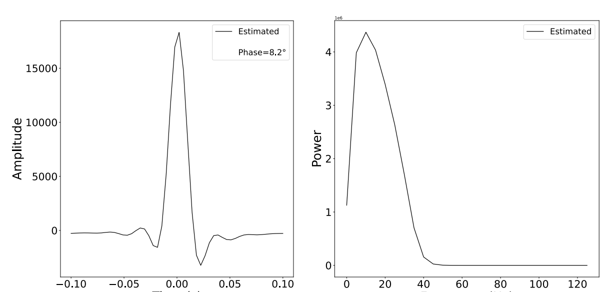

Fig. 9. Estimated wavelet (via IFFT) and spectrum. The model recovers a low-frequency-dominated spectrum with phase $8.2°$.

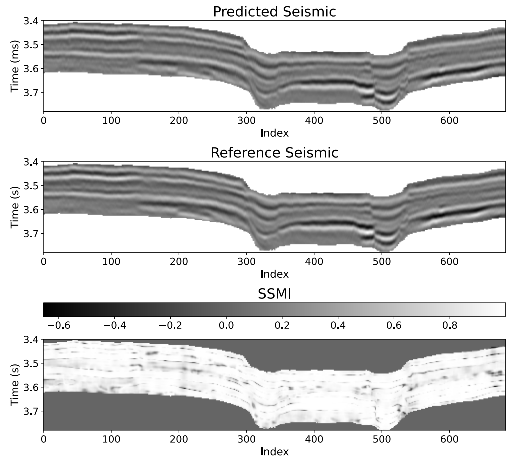

Fig. 10. Predicted vs. real seismic data and structural similarity (SSMI). The model achieves $M\text{-}SSIM = 0.75$ within the zone of interest, indicating consistency with physical constraints.

wavelets, producing synthetic seismic data with high similarity to the observed data.

The predicted impedances exhibit limited lateral continuity, likely due to the use of 1D convolutions, which could be addressed with 2D architectures or post-processing. Although the estimated wavelets are realistic, further comparison with traditional extraction methods is needed to better assess limitations. Future work includes integrating the model into automated well-tie workflows, leveraging its ability to jointly estimate impedance and wavelet directly from seismic data.

References

[1] M. Li, X. song Yan, and M. zhao Zhang, *A comprehensive review of seismic inversion based on neural networks*, Dec. 2023. DOI: 10.1007/s12145-023-01079-4.

[2] C. R. Marques, V. G. dos Santos, R. Lunelli, M. Roisenberg, and B. B. Rodrigues, "Analysis of deep learning neural networks for seismic impedance inversion: A benchmark study," *Energies*, vol. 15, no. 20, p. 7452, Oct. 2022, ISSN: 1996-1073. DOI: 10.3390/en15207452. [Online]. Available: http://dx.doi.org/10.3390/en15207452.

[3] G. E. Karniadakis, I. G. Kevrekidis, L. Lu, P. Perdikaris, S. Wang, and L. Yang, *Physics-informed machine learning*, Jun. 2021. DOI: 10.1038/s42254-021-00314-5.

[4] Z. Hao et al., *Physics-Informed Machine Learning: A survey on problems, methods and applications*, Nov. 2022. [Online]. Available: https://arxiv.org/abs/2211.08064#.

[5] Y. Su, D. Cao, S. Liu, Z. Hou, and J. Feng, "Seismic impedance inversion based on deep learning with geophysical constraints," *Geoenergy Science and Engineering*, vol. 225, p. 211 671, Mar. 11, 2023. DOI: 10.1016/j.geoen.2023.211671. [Online]. Available: https://doi.org/10.1016/j.geoen.2023.211671.

[6] A. Kazemi, "A comprehensive review of computer vision for reservoir modelling and data assimilation," *Discover Applied Sciences*, vol. 7, no. 12, Nov. 24, 2025. DOI: 10.1007/s42452-025-07743-2. [Online]. Available: https://doi.org/10.1007/s42452-025-07743-2.

[7] P. Li, M. Liu, M. Alfarraj, P. Tahmasebi, and D. Grana, "Probabilistic physics-informed neural network for seismic petrophysical inversion," *Geophysics*, vol. 89, pp. M17–M32, 2 Mar. 2024, ISSN: 19422156. DOI: 10.1190/geo2023-0214.1.

[8] M. Alfarraj and G. AlRegib, "Semisupervised sequence modeling for elastic impedance inversion," *Interpretation*, vol. 7, no. 3, SE237–SE249, Jun. 2019. DOI: 10.1190/int-2018-0250.1. [Online]. Available: https://doi.org/10.1190/int-2018-0250.1.

[9] P. Li, D. Grana, and M. Liu, "Bayesian neural network and Bayesian physics-informed neural network via variational inference for seismic petrophysical inversion," *Geophysics*, pp. 1–46, Jul. 2024. DOI: 10.1190/geo2023-0737.1. [Online]. Available: https://doi.org/10.1190/geo2023-0737.1.

[10] C. Sakar, N. Schwartz, and Z. Moreno, "Physics-Informed neural networks trained with Time-Lapse Geo-Electrical tomograms to estimate water saturation, permeability and petrophysical relations at heterogeneous soils," *Water Resources Research*, vol. 60, no. 8, Aug. 2024. DOI: 10.1029/2024wr037672. [Online]. Available: https://doi.org/10.1029/2024wr037672.

[11] H. Zhao, Y. Hao, W. Xu, and C. Li, "Adaptive-sampling physics-informed neural network for viscoacoustic wavefield simulation," *IEEE Geoscience and Remote Sensing Letters*, vol. 21, pp. 1–5, 2024. DOI: 10.1109/LGRS.2024.3418814.

[12] M. Rasht-Behesht, C. Huber, K. Shukla, and G. E. Karniadakis, "Physics-Informed neural networks (PINNs) for wave propagation and full waveform inversions," *Journal of Geophysical Research Solid Earth*, vol. 127, no. 5, Apr. 2022. DOI: 10.1029/2021jb023120. [Online]. Available: https://doi.org/10.1029/2021jb023120.

[13] J. Dvorkin, M. A. Gutierrez, and D. Grana, *Seismic reflections of rock properties*. Cambridge University Press, Mar. 2014.

[14] G. S. Martin, R. Wiley, and K. J. Marfurt, "Marmousi2: An elastic upgrade for Marmousi," *The Leading Edge*, vol. 25, no. 2, pp. 156–166, Feb. 2006. DOI: 10.1190/1.2172306. [Online]. Available: https://doi.org/10.1190/1.2172306.

[15] A. J. Bet, *Joint seismic inversion and wavelet estimation using physics-informed neural networks*, https://github.com/anthony-bet/Joint-Seismic-Inversion-and-Wavelet-Estimation-Using-Physics-Informed-Neural-Networks, 2026.